Experimental and Computational Studies on Flow Behavior Around Counter Rotating Blades in a Double-Spindle Deck

Woochong Chon*
Nuclear Safety Analysis Department, Korea Nuclear Fuel Co. Ltd, 493 Deokjin-dong, Yuseong-gu, Daejeon 305-353, Korea
Ryoichi S. Amano
Dept. of Mechanical Engineering, University of Wisconsin-Milwaukee, PO Box 784, Milwaukee, WI 53201, U.S.A.

Experimental and computational studies were performed to determine the effects of different blade designs on a flow pattern inside a double-spindle counter rotating mower deck. In the experimental study, two different blade models were tested by measuring air velocities using a forward-scatter LDV system. The velocity measurements were taken at several different azimuth and axial sections inside the deck. The measured velocity distributions clarified the air flow pattern caused by the rotating blades and demonstrated the effects of deck and blade designs. A high-speed video camera and a sound level meter were used for flow visualization and noise level measurement. In the computational works, two-dimensional blade shapes at several arbitrary radial sections have been selected for flow computations around the blade model. For three-dimensional computation applied a non-inertia coordinate system, a flow field around the entire three-dimensional blade shape is used to evaluate flow patterns in order to take radial flow interactions into account. The computational results were compared with the experimental results.

Key Words: Experimental Investigation, Computational Fluid Dynamics (CFD), Laser Doppler Velocimetry (LDV), Lawn Mower, Rotating Blades, Flow Behavior

Nomenclature

D_d : Diameter of deck
$\mathbf{g}$: Gravitational acceleration vector
H_1 : Height of deck
H_2 : Gap between deck and table
k : Turbulent kinetic energy
L_b : Length of blade
L_d : Length of deck
N : Rotational speed
p : Instantaneous pressure
R : Blade radius
$\mathbf{r}$: Position vector
r : Tested point radius
U : Mean velocity component
u_i : Fluid velocity in the ith direction
u' : Fluctuating velocity
$\overline{u_i' u_j'}$: Reynolds-stress
$\mathbf{v}$: Liquid velocity vector
$\mathbf{v}_r$: Relative velocity vector
V : Tangential velocity
V_{max} : Velocity of blade tip (Maximum velocity of blade)
V_z : Axial velocity
Z : Distance from blade to housing on axial direction
z : Distance from blade on axial direction

* Corresponding Author,
E-mail : wchon2000@yahoo.com
TEL : +82-42-868-1849; **FAX** : +82-42-863-4430
Nuclear Safety Analysis Department, Korea Nuclear Fuel Co. Ltd, 493 Deokjin-dong, Yuseong-gu, Daejeon 305-353, Korea. (Manuscript **Received** March 11, 2003; **Revised** April 1, 2004)

x : Cartesian coordinate
δ : Unit tensor
ε : Dissipation rate of turbulence kinetic energy
μ : Molecular viscosity
μ_t : Turbulent viscosity
π : Total stress tensor
ρ : Density of fluid
τ : Shear stress
τ_{ij} : Stress tensor
$\boldsymbol{\Omega}$: Angular velocity vector
ω : Angular velocity of blade

Subscripts

i, j, k : Tensor notations

Superscripts

$-$: Time-average values
$'$: Turbulent fluctuation

1. Introduction

The aerodynamics of a rotating blade is an important research area for the improvement of design in hover crafts, VTOL, and other industrial applications such as lawn mowers, fans, blowers, snow blowers, etc. Understanding of the mechanisms of aerodynamics of a rotating blade is one of the challenging research topics. To date, many of the designs for such blades have depended upon experience through numerous trials. Trial and error procedures are time-consuming and high cost. Therefore, the flow patterns near a rotating blade are not well understood, and it is difficult to explain the complete fluid dynamic characteristics occurring in lawn mowers. Lawnmower blade and deck designs must allow for maximum airflow and re-circulation of the grass clippings for better mulching. The flowfield around a rotating blade significantly affects the blade failures, vibrations, and associated noise and other adverse factors. In order to accomplish this, modifications must be made to the blade profile and cutting angles. In addition, proper mower deck layouts and geometries need to be tested to verify their airflow potential. The wider and higher upward air velocity at the tip of the blade makes the better cutting performance since most of grass cutting is occurred at this area. Clearly, there is a need for investigations to help mower designers optimize the configurations of blades and decks, and improve cutting performance.

The objectives of this study are to experimentally and computationally observe the effects of different blade configurations on the flows generated in a mower housing, and to develop a flow simulation that can predict improved designs. This database can be used for aerodynamic studies in turbomachinery and other aerodynamic applications. For these reasons, measurements of the velocity field around rotating blades in a housing, and computational simulations of blades and the mower deck, have been performed in this study. Additionally, high-speed video footage was taken to gain further insight into the flow conditions within the housing. Lawn mower is to be classified into two types. One is single rotating blade type, which is used for walk-behind mowers or compact size tractor mowers, and the other is multi-rotating blades type, which is applied for large scale tractor mowers. The single rotating blade type is generally used for home appliances. The multi-rotating blades type mower uses double or triple spindle in a single deck to extend grass cutting area. The double spindle mower can be divided into two classes, which are counter-rotating blades for mulching grass clipping type and co-rotating blades for side discharge type. The side discharge type mower generally has a bag installed in discharge area to collect grass clipping. A model tested for current research is a type of double spindle, counter-rotating mulching deck, which is the most common and widely used mower deck on the market and has almost no open research literatures available.

The flow inside a mower housing is a two-phase flow of a gas-solid particle system (air-grass clippings) similar to cyclones, separators, dust collectors, snow drifts, etc. The grass clippings circulate with air inside the mower housing after being cut. The flow pattern of grass clippings was carefully investigated for the mulching mower deck, since clipping size and motion are important factors for lawn mower performance. The

blades tested for current research are designed in such a way that the angle of attack varies along the radial direction. This design creates complicated flow patterns inside the deck.

2. Experimental Set-Up

The experimental facility consists of a deck model, a running motor, pulley and v-belt system, a power supply, automatic cut-off switch system, a velocity measuring system (LDV), LDV traversing system, two particle generators, and a data acquisition system. Figure 1 shows the schematic diagram of experimental set-up with LDV system.

The flow pattern inside the housing was observed by using a TSI Laser Doppler Velocimetry (LDV) system. Collection of data was performed at several different azimuth and axial sections of the deck. In conjunction with the velocity measurements, a high-speed video camera was used to observe the flow pattern caused by the blade rotation. Then a sound level meter was used to measure the noise level generated by the running mower deck blades.

Figure 2 shows the schematic diagram of the tested mulching mower deck. This model is a double-blade counter-rotating deck with a double housing design that was 1.076m wide. The dimensions are listed in Table 1. The housing is specially made of clear plastic for flow visualization and LDV experimentation. The deck model is installed on the test stand and powered by a 5 hp AC motor (230Volt, 3450rpm). The test stand (0.9m×2.0m) was constructed from plywood with a steel frame. To allow for the vertical

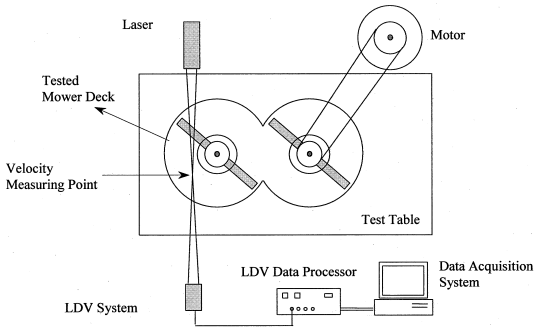

Fig. 1 Schematic diagram of experimental set-up

Table 1 Dimensions of tested deck and blade

Symbol	Dimension	Symbol	Dimension
D_d	0.575m	L_b	0.574m
L_d	1.076m	V_{max}	76m/s
H_1	0.102m	N	2700rpm
Z	0.082m	R	0.287m

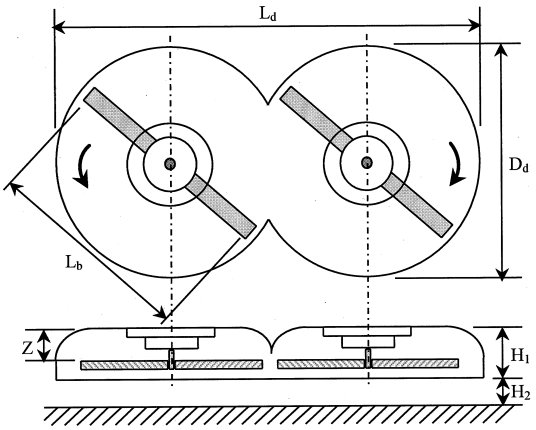

Fig. 2 Schematic diagram of mower deck

and horizontal positioning of the mower deck, four sliding bracket assemblies were designed and installed on the test table. Each assembly includes a sliding flat bar and an L bracket. The L brackets connect the mower to the flat bar pieces and allow the mower to move vertically. The height between the test table and the bottom of the mower deck is adjustable, from 0.025m to 0.10m. The flat bar pieces are set in the test stand and allow the L brackets to move horizontally. The rotational speed of the blade is set at 2700rpm by using a belt-pulley system. The motor and pulley mounting brackets were also designed to allow for the proper vertical and horizontal placement of the motor. The running belt guard was manufactured of a 0.64cm wood plate and a flexible steel plate to increase safety during the high-speed experiment. The artificial grass mat is attached on the test table to simulate the working condition of the lawn mower in a field test case. The LDV system is also installed on a movable traversing system to provide variable positioning, horizontally and vertically. The crank design of the traversing system is able to improve adjus-

tments in both x and y directions of the horizontal plane. The support stand was fitted with two units, to make vertical and horizontal adjustments.

Two particle generators were installed underneath the test table to supply seeding for the LDV test. The data obtained during this experiment was corrected and saved in the data acquisition system.

3. Experimental Procedure

The blade for the mulching type mower deck has two opposite inclinations at each side. Two kinds of blades were tested under the same experimental conditions. Figure 3 shows the schematic diagram of the tested two blade models. The blades are designed in such a way that the angle of attack varies along the radial direction. The purpose of the change in slope is to cause a flow around the blade in both upward and downward directions to help air circulation inside housing since mulching type mower deck does not have air discharge area on housing. The angle at the tip of the blade is designed to make higher upward velocity whereas the opposite angle near the middle section of the blade is designed to help downward velocity generation. This air flow pattern is expected to induce low pressure at the rotating blade center and helps higher upward velocity at the tip of the blade for better grass mulching performance.

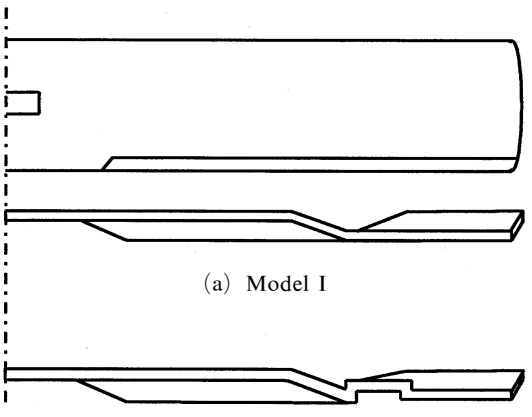

Fig. 3 Schematic diagram of two different blade models

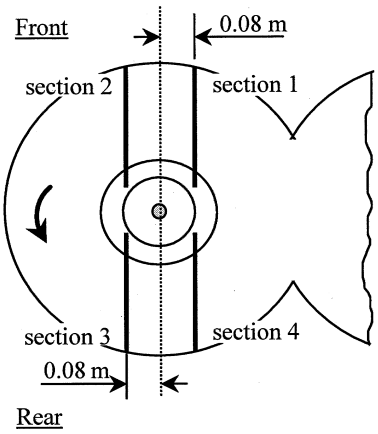

Fig. 4 Tested sections for LDV measurement

Model II blade, which is designed after several tests and geometry modifications, has a wavy curved portion at 0.62R from the center of the blade. Several cross sections shown in Fig. 4 were chosen to collect data. Each side of the housing is assumed to be symmetric since the blades are counter rotating (see Fig. 1). Hence, only one side of the deck was selected for the LDV measurement.

Tangential and axial velocities were measured at several different axial height positions. The three different gaps between the test table and the deck, $H_2/H_1=0.374$, 0.623, and 0.872, were tested to observe the affects of different heights in this study. The velocity data was collected and processed in the data acquisition system. This system will display a realtime probability distribution function (PDF) histogram of the particle velocities, and a statistical analysis of the sample taken, including the number of points taken, velocity mean, standard deviation, turbulence (%), a skewness coefficient, and a flatness coefficient. The data can be stored on a computer disc and retrieved for viewing or printing. Some preliminary test runs with the lawn mower were conducted to determine the proper settings for the data processor, which would be kept constant throughout most of the tests. For each set of test conditions, the test section was positioned to pass through the center of the probe volume and intersect the optical axis, within the plane of the

intersecting laser beams. The realtime PDF was viewed while the mower was running to assure that the processor settings were appropriate. When it was determined that the mower, processor and software were all functioning properly, and adjusted correctly, a sample of 6000 data points was taken and stored. These data were later analyzed and displayed as a PDF histogram and a table of available statistics for each set of test conditions.

In summary, each measurement was taken at the horizontal test section inside the mower housing. All of the data for each sample is available in its PDF data file and displayed in the PDF histogram. The LDV graphs were produced using the average velocity in each sample. Flow visualization was also performed using a high-speed video camera, and noise levels were measured using a sound level meter.

3.1 LDV System

The LDV is a well established technique used in fluid flow research as a non-invasive method for obtaining velocity and turbulence information in a variety of applications including separated flows, liquid flows, high turbulence intensity flows, high temperature flows, variable property flows (non-isothermal), rotating machinery, combustion, very low velocity flow, etc.

A 1980 TSI model LDV system was used to measure the air velocities inside the housing. The LDV system consists of several pieces of equipment, including a laser source, optic system (beam splitter, focusing lens, collecting lens, bragg cell and photo multiplier tube), signal processor, and a data processor. The LDV has several optic system modes including reference beam mode, dual beam mode, one beam mode, and fringe mode. The laser passes through the transmitting optics and the light beams intersect at a point creating a probe volume through which the seeding particle passes inside the mower housing. The scattering two doppler shifted light signals that pass through the receiving optics are heterodyned in the photomultiplier. The different frequencies are sent to the data processor, which validates the signal and can send the processed data to a compatible data collection device.

The LDV system used in this experiment has one component and a dual beam mode system, powered by a 30mW maximum output He-Ne ion laser. There are three types of scattered light collection, back scatter, forward scatter and off-axis. The forward scatter method was chosen in this study to increase intensity.

3.2 Seeding

The LDV measures the velocity of particles traversing the measured volume, but not the air molecules, so seeding the flow field must also be performed. In most air flows, naturally present particles that can generate good signals are not sufficient in number. Particles in the test room with greater than 0.5 microns of diameter have a number density (number/c.c.) typically less than 1. This means that the probability of having a particle in the LDV measuring volume (e.g. 100 microns$\times$1,000 microns) is very small. Hence, in most of the air flows, there is a need to seed the flow with appropriately sized particles. The optimum seed particles are small enough to follow the flow and large enough to generate a sufficient amount of scattered light. In general, the use of a water-glycerine mixture, or of oils (vegetable oils, mineral oils, DOP and other liquids), are common to seed gas flows. In some cases, solid particles such as PSL, silicon beads and kaoline have been used for seeding gas flows. Salt and sugar have also been used as seeds by atomizing the solutions and then drying the droplets. In these cases, the seed particle size is controlled by adjusting the concentration of the solutions. Small particles for forward scatter applications have been generated in this fashion.

The frequency response is a function of the particle diameter and density. In general, a particle with a small, aerodynamic diameter would be a good choice as the seed for high speed flows. As the diameter gets smaller, SNR could be maximized by reducing the measuring volume and increasing the laser power. Small solid particles such as PSL and TiO_2 have been used to seed high speed flows. A solution of solid particles in an evaporating medium is atomized to

control the seed particle size. Droplets of atomized liquids such as silicone oils, and Dow Corning 704 have been used as seed particles. One problem with using the laser velocimetry in flows containing regions of high vorticity is that the seeding particles will not precisely follow the trajectories of fluid elements because they tend to spin out from the measuring section due to the centrifugal effects. Another problem is that the deck model has clearance between the housing and the test table. Therefore, the particles used should be harmless to humans. Tests were performed by supplying atomized water droplets from ultrasonic nozzles. Water droplets are continuously supplied from two nozzles installed underneath the test table.

3.3 High-speed video camera

The flow patterns were observed by using a high-speed video camera. A high-speed video taping method offers valuable insight into the global flow patterns within the mower deck and is useful to compare the performance of different blades. For the experiments with the high-speed camera, footage was recorded at several different angles. The NAC color High Speed Video HSV-1000 FPS camera V-054 was used. The camera has the ability to record up to 14 minutes of high speed motion at 1,000 frames per second, on a standard color SVHS cassette. For added versatility the system is easily switched to monochrome operation for those times when a black and white image is more appropriate. The complete system consists of a video tape recorder (VCR) and a video monitor, mounted on an integral card, and the HSV-1000 color camera. An easy-to-use, hand held keypad controls all record and playback functions. The camera also has record and playback controls on its rear panel. The recording speed is adjustable at either 500 or 1, 000 frames per second with variable shutter speed to helps capture sharper pictures. The system has switchable recording formats for either Super-VHS or VHS, with a resolution of 350+ horizontal TV lines. The monitor has a 750+ horizontal line resolution and the camera has a 400+ line video resolution. After the taping session is over, the footage can be played back at any speed or slowed to a still position through a rotary control for a frame by frame analysis. Two different blade models were taped and compared at the same running conditions. Video taping was performed for several different angles of view throughout the deck. Coalescence of small pieces of paper, the Confetti Test, was also observed by video taping the flow motion.

(1) Confetti Test

The first high-speed camera experiment performed was the Confetti Test to visualize grass clipping flow path. The similar size and weight Confetti with grass clipping were selected to make better visualization since Confetti has higher intensity of light than grass clipping. The camera was placed at several different positions on the deck while small paper clippings were fed into the mower deck from the bottom of the test table. The particle flow of the paper clippings was observed as they traveled around the path inside the deck. The frames of the images were simulated in a computer so that distributions of the small pieces of paper could be easily observed.

(2) Tuft Test

0.04m strings were attached on the inner wall of the deck during high-speed video taping. The purpose of using the Tuft Test was to observe the unpredictable flow patterns inside the deck housing. Suction, blowing, and turbulence are the main flow characteristics that need to be controlled for designing a good performance mower deck. Figure 5 shows the views of tuft test for overall and partial views. Figure (b) also shows the strings aligned with air flow direction with rotating of blade.

3.4 Sound level meter

Noise levels were measured with a Bruel & Kjaer Precision Sound Level Meter Type 2203 for three different cases, one without blade, the second with blade Model I, and the third with blade Model II (see Fig. 3). The sound level meter was calibrated by using the sound level calibrator Type 4230 before each measurement. This cali-

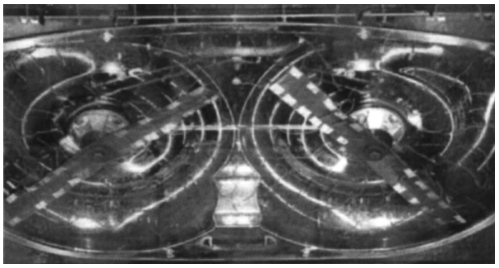

(a) Overall view

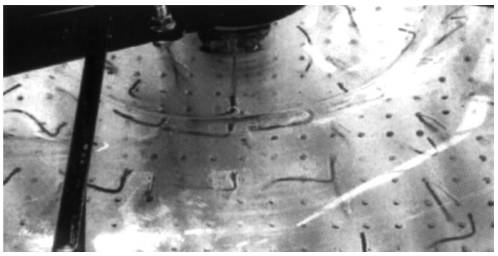

(b) Partial view

Fig. 5 Views of tuft test using high-speed video camera

brates the meter at 1000Hz (±2%) and thus is independent of the weighting networks. After calibration it is possible to perform sound level measurements to an accuracy of ±0.3dB with the Precision Sound Level Meter Type 2203. The influence of static pressure is very small, thus the calibration signal is virtually independent of barometric pressure or altitude, for ordinary use. The calibration may also be regarded as independent of temperature for most applications. The tests were performed at several different locations under the same conditions. The measured values were averaged and recorded.

4. Experimental Uncertainty

If it is assumed that the LDV system is measuring on a real doppler burst. The error in the counter measurement of time is 0.25% at 20MHz. The digital data system uses 10 binary bits, for approximately 0.25% accuracy. The beam angle was measured by TSI and specified to 0.1%. The total error of a doppler burst measurement is therefore approximately 0.6%, an extremely small value.

There is also some influence of velocity bias on the measurement. Velocity bias occurs because more high-velocity particles go through the measurement volume than low-velocity particles. The data was screened at standard deviations, and only about 0.4% of the data points were rejected out of 6,000 in the experiments.

The source of error with the greatest potential for causing uncertainty is the measurement of noise instead of doppler bursts. The system and counter setup were checked so that no-particle-seeding corresponded to a zero data rate. It was also found useful to block the beam and make sure that the data rate went to zero. Generally, measurements made on noise fall considerably from doppler burst measurements. The LDV data confirms that there is little problem with bad, noise-based measurements in the current data.

The 632.8nm laser line was used for both tangential and axial velocity components. The components were measured independently. Seed particles of ultrasonic nozzle (~20μm diameter) were added to the fluid to provide acceptable data rates. Six thousand data points were taken at each position to determine the local mean velocity. Between 1,000 and 10,000 data points were averaged, and it was discovered that results were independent for sample sizes over 4,000 data points.

Another error was introduced by the uncertainty of the traversing mechanism. The traversal resolution in the three directions was ±0.2μm with a placement precision of 0.5mm/m.

5. Numerical Model

The numerical method used for this research is the three-dimensional finite volume difference (FVD) method with a QUICK[12] scheme for descretization of convection-diffusion terms and SIMPLEC[13] for pressure computations. The turbulence model employed for the computations is the standard k-ε with the wall-function model for the wall boundary conditions.

Two computational models have been developed and combined with the computational code to better describe the aerodynamics of lawn mowers. First, two-dimensional blade shapes at

several arbitrary radial sections were selected for flow computations around the blade model. Each cross section of the blade, drawn with CAD software, was modeled for the flow computations. These blade cross sections were transported into the CFD code developed at the CFD laboratory of University of Wisconsin-Milaukee, and computed for flow behavior analyses. Second, the data obtained from these analyses were used for computations of the three-dimensional deck model.

5.1 Governing equations

The governing equations needed to simulate a fluid flow field of the rotating blade are the conservation equations of mass and momentum, expressed in the vector forms shown below.

$$\nabla \cdot \rho \mathbf{v} = 0 \tag{1}$$

$$(\mathbf{v} \cdot \nabla)\rho \mathbf{v} = -\nabla \cdot \pi + \rho \mathbf{g} \tag{2}$$

In these equations, ρ is the air density, $\mathbf{v}$ is the air velocity vector, $\mathbf{g}$ is the gravitational acceleration vector, and π is the total stress tensor of the air. And π is given by:

$$\pi = p\delta + \tau \tag{3}$$

where, p is the static pressure, τ is the stress tensor of air, and δ is the unit tensor. The above governing equations are valid for both laminar and turbulent flows. The following is the corresponding components in summation convection for repeated indices. The continuity equation is given by:

$$\frac{\partial(\rho U_i)}{\partial x_i} = 0 \tag{4}$$

The momentum equation is given by:

$$\frac{\partial(\rho U_i U_j)}{\partial x_j} = -\frac{\partial p}{\partial x_i} + \rho g_i + \frac{\partial \tau_{ij}}{\partial x_j} \tag{5}$$

where τ_{ij} is the stress tensor, and g_i is the gravitational acceleration in the ith direction.

Since the velocities of the flow in a lawn mower are small compared to the sound velocity, it can be assumed that the flow is incompressible. Thus, equations (4) and (5) reduce to:

$$\frac{\partial U_i}{\partial x_i} = 0 \tag{6}$$

and

$$\rho \frac{\partial}{\partial x_j}(U_i U_j) = -\frac{\partial p}{\partial x_i} + p g_i + \frac{\partial \tau_{ij}}{\partial x_j} \tag{7}$$

where $\tau_{ij} = \mu\left(\frac{\partial u_i}{\partial x_j} + \frac{\partial u_j}{\partial x_i}\right) - \rho\overline{u_i' u_j'}$ (8)

In equation (8), the term $-\rho\overline{u_i' u_j'}$ is referred to as the Reynolds stress.

For computations of turbulent flows, the standard $k-\varepsilon$ model has been widely used for many applications. This is partially because it is relatively simple and has been proven to provide engineering accuracy for a variety of turbulent flows, including shear flows and wall-bounded flows. In addition, the $k-\varepsilon$ model is semi-empirical since its constants are taken from simple, steady and high Reynolds flow experiments.

The $k-\varepsilon$ turbulence model is an eddy-viscosity model. The Reynolds stresses are assumed to be proportional to the mean velocity gradients, with the constant proportionality being the turbulent viscosity μ_t assumed to be isotropic and to play the same role as the molecular viscosity μ. At wall boundaries, the wall functions are used near the wall region to estimate the effects of the wall on turbulent flows. These functions are empirical and are used in lieu of solving the entire turbulent boundary layer.

In each iteration, several steps are executed. At the first step, the U, V and W momentum equations are each solved in turn using the guessed values for pressure in order to update the velocity field. Since the velocities obtained in the first step may not satisfy the mass continuity equation locally, a "Poisson-type" equation is derived from the continuity equation and the linearized momentum equations. This 'pressure correction' equation is then solved to obtain the necessary corrections to the pressure field. Corresponding adjustments to the velocity components are also made. The $k-\varepsilon$ equation is solved using the updated velocity to obtain the distribution of the effective viscosity for turbulent flow. Any auxiliary equations are solved using the previously updated values of the other variables and

the fluid properties are also updated. Finally, a check is made to see if equation sets converge. These steps are continued until the sum of the residuals in each equation, within each finite control volume, is less than a preset value, which means that the convergence results are obtained.

5.2 Two-dimensional model

One of the advantages of using a two-dimensional blade model is that the local flow behavior and the effect of the blade geometry perimeters on the entire flow characteristics near the blade can be observed more easily than with three-dimensional models. Moreover, two-dimensional models are less complicated and require less CPU time than three-dimensional approaches. Therefore, it was decided to start with a two-dimensional model to get some insight before moving on to three-dimensional models.

Before making the numerical computations, it is required to generate the correct geometry of the model and the reasonable grids. The method and procedure of generating geometry and grids discussed below are valid for a two-dimensional model.

Three cross sections of the blade were chosen for calculation. The distances from each cross section to the rotating axial line of the blade are 0.15m, 0.19m and 0.24m, respectively. The cross section views of two different blades are shown in Fig. 6. With the blade spinning at 2700RPM the tip of the blade is moving at 76m/s. In this manner the inlet velocity conditions were evaluated based on this rotational speed at each radial section. The input velocities obtained from angular velocity for different cross sections of blade are shown in Table 2.

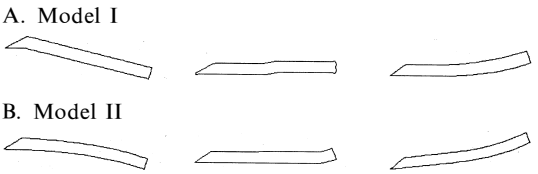

(a) Section A (R=0.15m) (b) Section B (R=0.19m) (c) Section C (R=0.24m)

Fig. 6 Cross section views of each blade model

Table 2 Input velocity for two-dimensional computation

Section	Radius(m)	Input Velocity(m/s)
A	0.15	42.39
B	0.19	53.69
C	0.24	67.82

$$V_{inlet}(m/s) = 2\pi\omega r/60 \quad (9)$$

A rectangular face with a dimension of 0.22×0.12m was added around the cross section view of the blade. The blade was located at the center of the rectangle and the 'velocity inlet' boundary condition, Vinlet, was given at the front rectangle edge of the blade cross section. Other rectangle edge behind blade was set as 'outlet' boundary condition and the other two edges were set as 'wall' boundary conditions.

In this study, the structured rectangular grid is used. The final grid for one of the two-dimensional blade models is shown in Fig. 7. The upper and lower sides of the rectangle outside of the blade, and the geometry of the blade cross section were defined as walls. Velocity inlet was used for the inlet boundary condition and static pressure inlet was used for the outlet boundary condition.

The flow is assumed incompressible due to its low Mach number condition. This process of data input includes defining physical constants such as the density of air, set at 1.177kg/m^3, and the viscosity of air at $1.846\times10^{-5}N.s/m^2$.

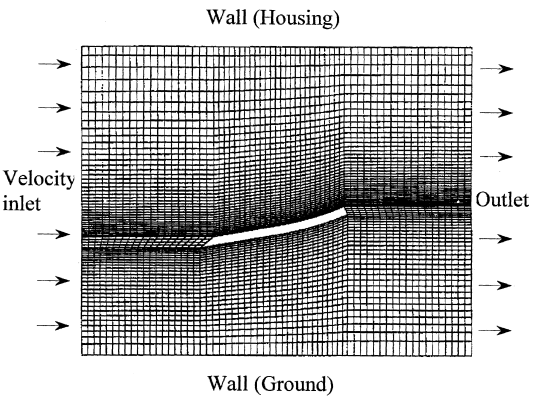

Fig. 7 Final grids for two-dimensional blade cross section C (Model II)

5.3 Three-dimensional model

In this model, a flow field around the entire three-dimensional blade shape is used to evaluate flow patterns in order to take radial flow interactions into account. To do this, the blade is at rest while the surrounding environment moves in a relative fashion. For this purpose, one quarter of the deck housing is employed as the solution domain of the model. The blade is located in the middle height position and at about 30° from the inlet of the computational boundary of the model. The lower side of the computational domain has been extended 0.064m all the way to the ground. This is the average height of the actual mower deck. The grid is generated by employing highly clustered meshes near solid walls. The total number of nodes is 75,000 for one side of the double compartments. The input velocities are provided along the blade surface while the flow along a gap between the ground and the deck housing is computed through the model. The same fluid properties were used as in the two-dimensional flow computations. Computations require approximately 10,000 iterations for the residuals to drop below 0.01% on a SGI Power Challenge Array at NCSA. Each computation takes about 4 hours of CPU time to achieve the above mentioned convergence criteria. The fully meshed three-dimensional model shown in Fig. 8 is based on the non-inertia coordinate system where the blade is stationary while the surrounding field including air, the deck wall, and the ground, rotates.

When the equations of motion are solved in an accelerating computational domain of reference, the acceleration of the fluid is augmented by the acceleration of the reference domain itself. In a rotating reference domain, this additional acceleration gives rise to the coriolis and centrifugal acceleration terms which appear in the revised momentum equations in the rotating domain :

$$\frac{D\mathbf{v}_r}{Dt}+2\boldsymbol{\Omega}\times\mathbf{v}_r+\boldsymbol{\Omega}\times(\boldsymbol{\Omega}\times\mathbf{r}) \qquad (10)$$

Here, $\mathbf{v}_r$ is the velocity in the rotating domain and is related to the velocity in the non-rotating domain, $\mathbf{v}$, as :

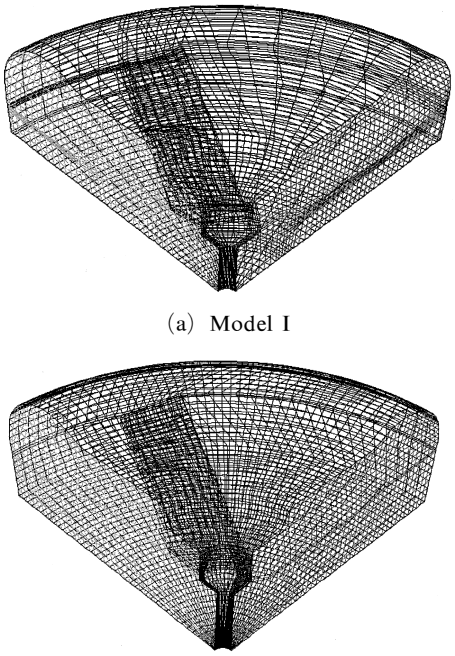

(a) Model I

(b) Model II

Fig. 8 Final grids for three-dimensional model

$$\mathbf{v}=\mathbf{v}_r+\boldsymbol{\Omega}\times\mathbf{r} \qquad (11)$$

where $\boldsymbol{\Omega}$ is the rotation vector and $\mathbf{r}$ is the position vector in the rotating domain. Three-dimensional model is solving the momentum equation in the form of (10) to predict the velocity $\mathbf{v}_r$ as defined by (11).

6. Results

The velocity measurements were taken at several different radial and axial sections inside the deck housing. The maximum measured velocities are listed in Table 3 and 4. The maximum tangential velocities usually occurred at r/R=0.51~0.73 from the center of the rotating shaft and maximum axial velocities usually occurred

Table 3 Maximum tangential velocity near the blade (m/s)

Section	1	2	3	4
Model I	15.38	14.38	15.88	14.52
Model II	17.99	17.95	18.39	16.11

Table 4 Maximum axial velocity near the blade (m/s)

Section	1	2	3	4
Model I	6.37	6.31	5.14	5.36
Model II	7.34	7.49	6.30	6.35

at r/R=0.76~0.84 from the center of the rotating shaft. This is because the velocities near the housing wall are reduced due to the wall friction. The velocity distributions at each section are not the same due to the fact that air suction varies from location to location.

6.1 Velocity distribution for model I

Figure 9 shows the tangential velocity distributions for Model I at several different heights for the measured points at four sections (see Fig 4). It was observed in these figures that the tangential velocity tends to increase from the center of the blade, up to r/R=0.52~0.59. Beyond that location, velocity decreases since the deck housing area is magnified and friction increases toward the outside wall. It is also observed in this figure that the velocity increases with the height of the measuring point in axial direction at both sections 1 and 3, whereas it decreases at sections 2 and 4. This occurs because of the change of air motion in the gap between the deck and the ground. Hence each section has a different air velocity layer.

6.2 Velocity distribution for model II

Figure 10 shows the tangential velocity distribution for Model II at the same points and sections as Model I in Fig. 4. The patterns of the velocity seem to be similar to that of Model I. However, the Model II blade generates a faster tangential velocity than the Model I blade in the whole field for the same blade speed and at the same positions. The velocities near the outer region are specially enhanced in Model II. The comparison of maximum tangential velocity between the two different blades is shown in Table 3. The pattern of the velocity at each section is the same.

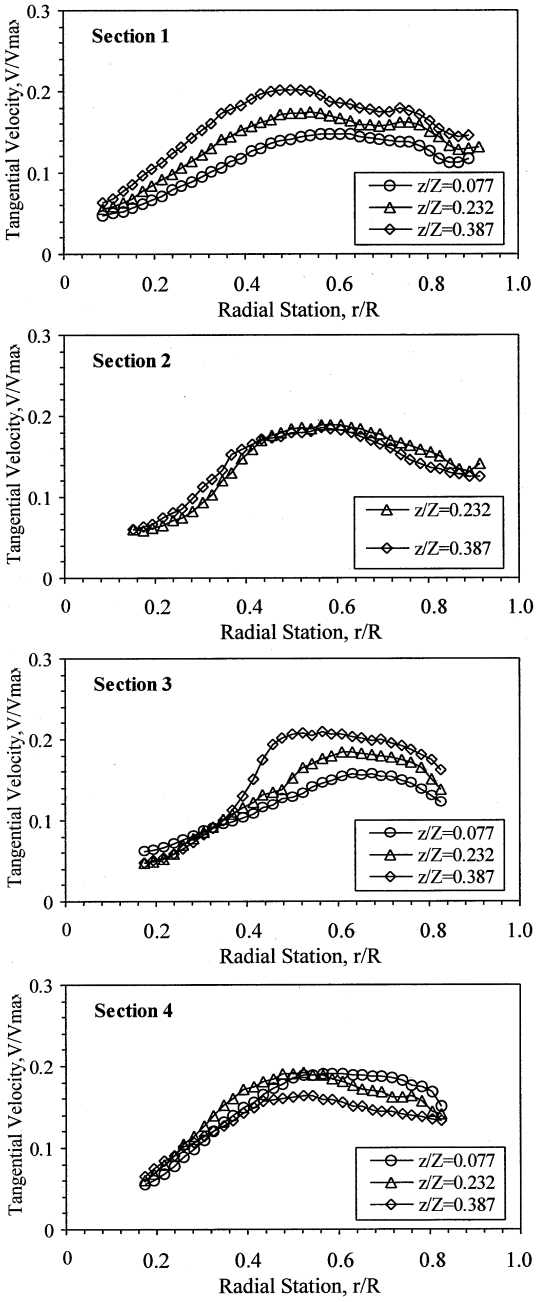

Fig. 9 Tangential velocity distribution for model I

6.3 Axial velocity distribution

The axial velocity was also measured at several different heights for the measured points at four sections the same as tangential velocity measurement but difference was relatively small. The axial velocity distributions for Model I and II are

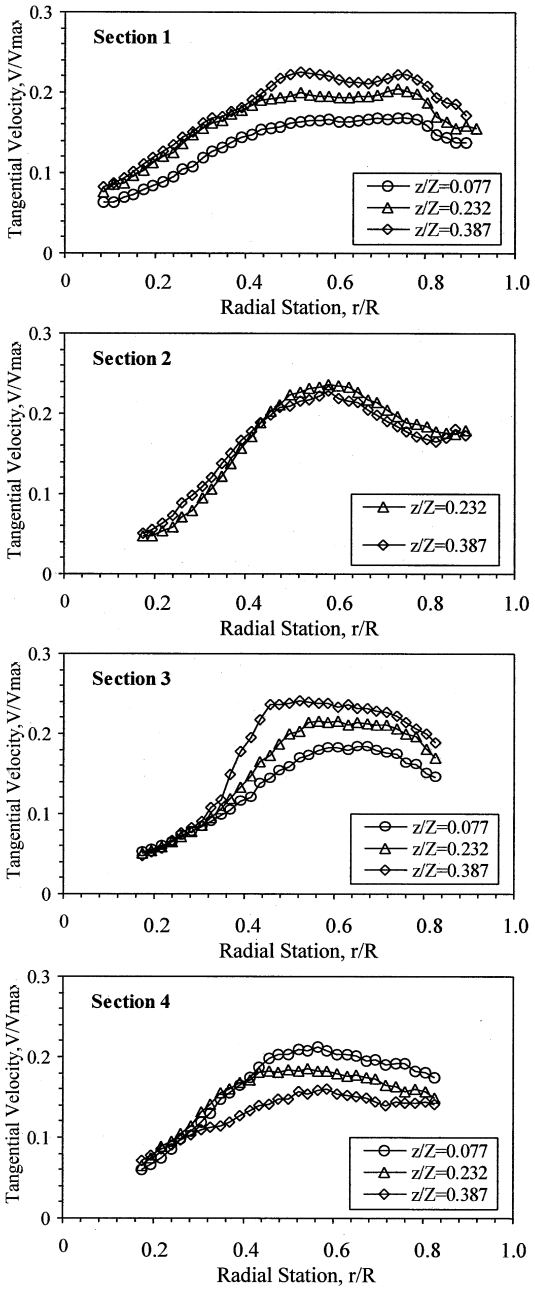

Fig. 10 Tangential velocity distribution for model II

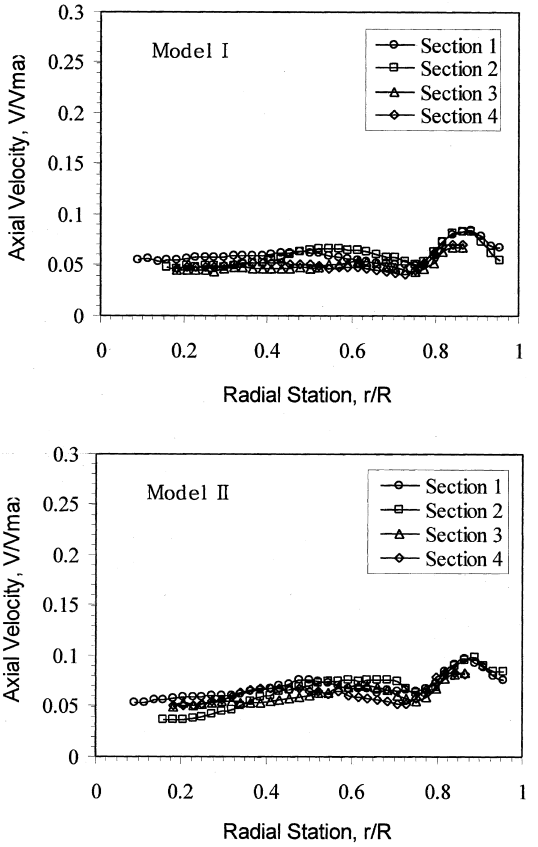

Fig. 11 Axial velocity distributions for model I and II ($z/Z=0.232$, $H_2/H_1=0.374$)

shown in Fig. 11.

In most of sections the velocity increases from the center of the blades to the perimeter of the mower deck. This trend is beneficial in that the higher upward velocities occur near the perimeter causing the lift of the grass before it is cut. This flow pattern improves the efficiency of the mower's mulching effect. Any grass that does not get cut by the first sweep of the blade has the potential to get cut in the following blade paths because they are stretched upward by the lift under the deck. The maximum velocity occurs around at $r/R=0.9$ and velocity decreases after that because of housing wall friction. The data also showed, on average, that the maximum axial velocity in the front area of the deck was higher than the velocity in the back area in the both blade models. This is also a beneficial velocity characteristic since the majority of the grass gets cut in the front of the deck.

The result also shows that only upward velocity is measured by experiments even blade has an opposite attack angle at the middle section to help air circulation inside housing. One of reason is that an axial velocity measurement is performed at about 0.02m above the blade plane because of

the restriction of LDV measurement. And the low pressure created by centrifugal force seems to be prevents downward velocity at the middle section. The mimum axial velocity was 5.4~6.4m/s for Model I and 6.5~7.5m/s for Model II. The axial velocity pattern is the same as other deck height (H_2) or measuring point height (z) for the same section.

6.4 Comparison for different deck height

Figure 12 shows the effect of height between ground and deck at section 1. The velocity at each height shows the same pattern: the maximum tangential velocity is almost the same at each section. This feature was also observed in the axial velocity distributions and at other sections. Hence it was found that the gap between the ground and the deck does not strongly affect the trend of the velocity.

6.5 High-speed video taping

High-speed video taping was performed to observe the air flow direction inside the deck housing by attaching threads on the wall inside the housing. Two blade models were tested with the same running conditions. In the first video taping experiment, small confetti was supplied through the hole of the bottom test table to observe the flow motion inside the housing while the blades are rotating. Most of the confetti pieces were fed into both the left and right sides of the deck where

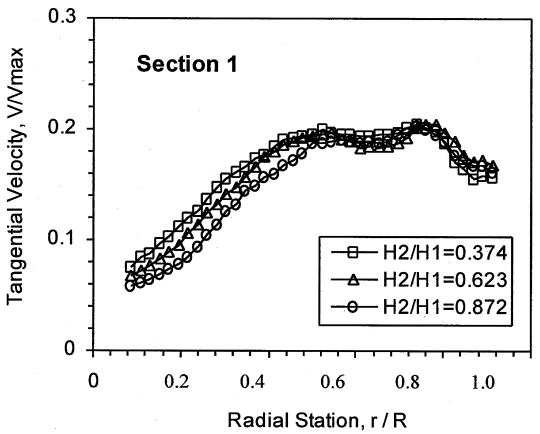

Fig. 12 Comparison of deck height for model II (z/Z=0.077)

Table 5 Noise test result

Blade Model	w/o blade	Model I	Model II
Noise Level	100db	120db	125db

air suction is present. Many of the pieces went around for several rotations and exited at the rear side of the deck. High turbulence motion was also observed at the center area of the deck. Blade Model II creates a wider suction area at both sides of the deck than Model I. The tuft test indicated strings aligning with the blade rotation direction except at the center area of the deck.

6.6 Noise test

The results of the noise test are listed in Table 5. The sound level meter was used at various locations in the deck, including a section between the two blades, and these noise levels were averaged. The average noise levels were 100dB without any blade installation and 120dB with blade Model I and 125dB with blade Model II. Hence each blade makes 20~25dB increments of noise. The noise level created by Model II is about 4.2% higher than Model I. The wavy curved portion of the Model II blade causes both faster flow and more resistance in the housing.

6.7 Computational results

Figure 13 shows the comparisons of the velocity vectors at different blade cross sections of each blade model. At cross section A, the sharp flow separation is occurred at the end of the sharp-ended point along the upper surface of the blade Model I. However it is almost disappeared in Model II. The curvature shape of blade Model II can generate more downward velocity than that of Model I. The flow pattern at the cross section B is uniform compared with other sections and two blade models make similar velocity distributions. At the views of cross section C, the rounded blade surface near the tip of the blade is intended to create lift force on the flow particles. However this rounded surface does not strongly effective in causing lifting force on the flow particles due to prior separation at the sharp edge. It also shows that Model II generates more upward velocity and

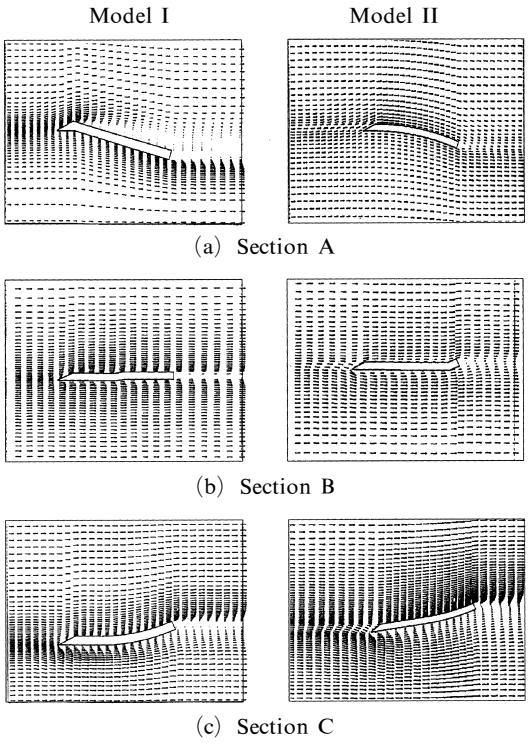

Fig. 13 Velocity vectors at different cross section of each blade model

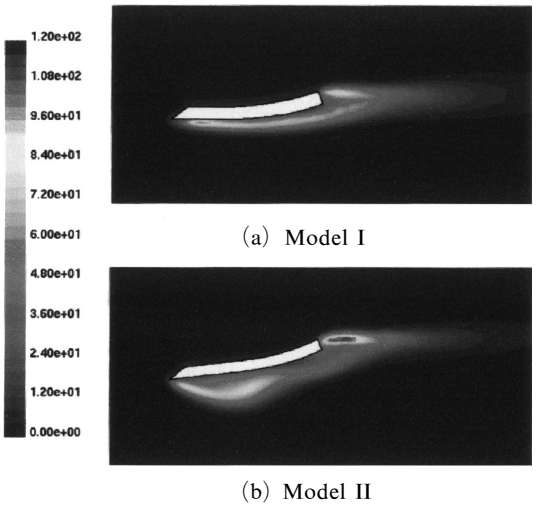

Fig. 14 Turbulent kinetic energy at cross section C (m^2/s^2)

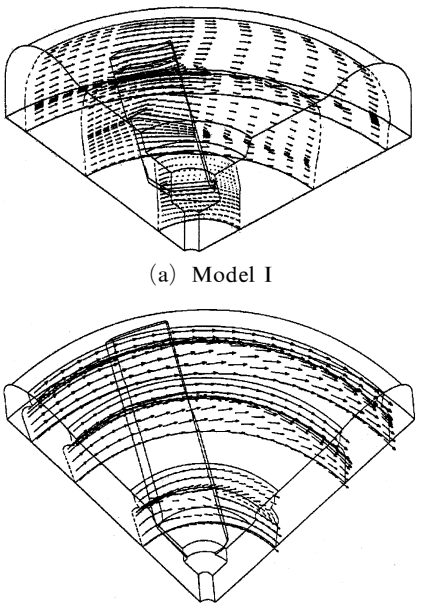

Fig. 15 Velocity vectors at different radial locations for three-dimensional model

flow separation tendency is smaller than those of Model I. However the difference is relatively small.

In other two-dimensional model results, high pressure occurs at the upper side of each blade cross section and low pressure occurs at the bottom of each blade. The highest pressure level occurs at the front edge of the blade. Blade Model II has a smoother velocity vector and a smaller turbulent zone than Model I in cross section A. The turbulent kinetic energy level is increased at cross section C for blade Model II since it has a deeper attack angle than that of Model I. The comparison of turbulent kinetic energy at cross section C is shown in Fig. 14.

Figure 15 shows the comparison of velocity vectors at different radial sections for three-dimensional model. It is found that the three-dimensional results seem to be relatively similar to the results obtained by using two-dimensional model calculations. Figure also shows that the downward velocity is occurred at the inner radial section since blade has an opposite attack angle near the inner section of the blade. However the effect is small and shown at or below the rotating blade plane since strong centrifugal force caused by high rotating speed makes low pressure at the inner section of blade. The experimental result discussed in Fig. 11 also shows only positive

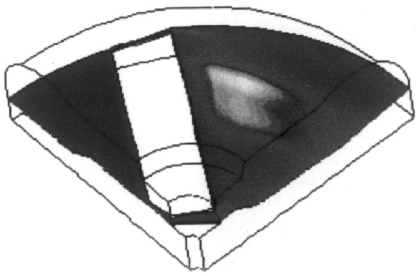

(a) Model I

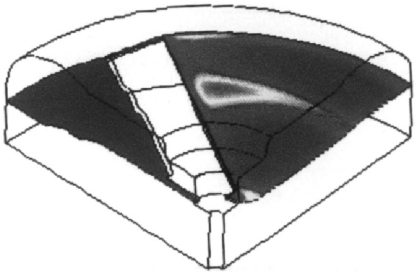

(b) Model II

Fig. 16 Computed turbulence level for three-dimensional model

upward velocity above the rotating blade plane.

Computed turbulence levels are shown in Fig. 16 for both blades in a three-dimensional model. As evidenced in this figure, the wavy curved portion in blade Model II generates higher concentrated turbulence wakes than blade Model I.

The velocity affects the inhalation power of flow particles in the flow motion field. Therefore, the inhalation power of the rotor motor can be increased by changing blade and housing designs. It should also be noted that in the case of increasing air velocities, turbulence intensity, and noise levels can also be increased. The bend created on blade Model II causes a faster flow and as a result, may create more resistance in the housing.

6.8 Comparison between computations and experiments

The four sets of experimental data have been compared with the computational results. The locations of those test data are shown in Fig. 4. Both experimental data and computed velocities at section 1 are compared and shown in Fig. 17 for Model I and Model II. In this figure it is noted

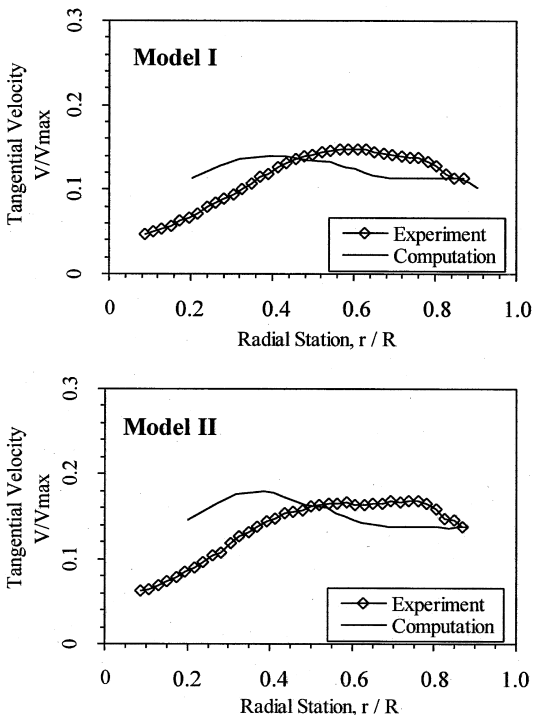

Fig. 17 Comparison of experimental result with computational result (Section 1, $H_2/H_1=0.374$)

that, although the maximum values of tangential velocity agree, the location of the computed maximum is predicted at $r/R=0.18$, while the experimental results have a maximum at between $r/R=0.25$ to 0.38. This discrepancy may be attributed to the fact that the computations cannot incorporate exact air flow conditions at the clearance between the housing and the ground. The clearance was fixed by pressure inlet boundary condition in computational domain. However the high-speed video in experimental test shows both in- and out-flow occur at the clearance around housing, simultaneously. Another reason of difference is that the computation is not considered the interaction of two rotating blades since three-dimensional model employ only one side of blade and one quarter of the deck housing.

7. Conclusions

Through this study, the experimental and com-

putational results have provided better understanding of the velocity patterns at each section and generated inside the mower deck during the operation. The observation via high-speed video taping gives a good opportunity for visual verification and comparison with the data obtained in the LDV test. The use of LDV system and a high-speed video along with the use of CFD code has given an opportunity to verify computational flows with visual experimental results. The experimental results have provided a good picture of what the velocity patterns at each section and inside mower deck look like. This information can be used in future designs of both mower decks and blades to achieve more desirable flow patterns.

After analyzing two different blade models, it was identified by both experimental and numerical studies that Model II, which has a wavy curved portion in the middle of the blade, performs better than Model I in enhancing the lifting effect inside the deck. It was observed that a wavy curved portion on Model II causes a higher turbulence level, which may result in higher noise and vibration levels. And experimental and computational results also can be used for explanation of the design effects of the blade and housing.

The computational calculations for the mulching type mower deck clearly show the flow pattern and other flow characteristics around the blade cross sections. Hence an optimum design for a mower blade can be found in consideration of the relation between better performance and lower turbulent energy. These results can provides a method of determining optimum values for critical design parameters before experimental validations for many other complicated rotating machinery designs.

Acknowledgments

Computations were performed using Power Challenge Array at NCSA (National Center for Supercomputing Applications) under grants NSF CTS960022N, CTS970032N, and CTS000003N. The authors are thankful to P. Wei, R.M. Achtner, D. Schwarz, G. Draxler, and F. Aldahshan who assisted with both the computations and the experiments.

References

American Standards Association, 1960, American Standard Safety Specifications for Power Lawn Mower.

Association for the Study of Flow Measurements, 1983, The Application of Laser Doppler Velocimetry, Japan.

Komerath, N. M. et al., R. B., 1985, "Velocity Measurements in the Near Field of a Rotor Blade in Hover," AIAA 3rd Applied Aerodynamics Conference, Colorado Springs, CO, AIAA-85-5013.

Rajan Menon and Wing T. Lai, 1991, "Key Considerations in the Selection of seed Particles for LDV Measurements," The 4th International Conference on Laser Anemometry, Cleveland, OH.

Mclaughlin, D. K. and Tiederman, W. G., 1973, "Biasing Correction for Individual Realization of Laser Anemometer Measurements in Turbulent Flows," *The Physics of Fluids*, 16, pp. 2082~2088.

Kwon, E. Y. and Cho, N. H, 2001, "Experimental Study on the Mean Flow Characteristics of Forward-Curved Centrifugal Fans," *KSME International Journal*, Vol. 15, No. 12, pp. 1728~1738.

Hoffman, J. D., 1993, Numerical Methods for Engineer and Scientists, McGraw-Hill Inc., New York.

Hinze, J. O., 1975, Turbulence, 2nd Edition, McGraw-Hill Inc..

Kang, S. H. and Zhang, Y. J., 2000, "Performance Prediction and Flow Field Calculation for Airfoil Fan with Impeller Inlet Clearance," *KSME International Journal*, Vol. 14, No. 2, pp. 226~235.

Launder, B. E. and Spalding, D. B., 1973, "The Numerical Computation of Turbulent Flows," *Imperial College of Science and Technology*, London, England, NTISN 74-12066.

Launder, B. E. and Spalding, D. B., 1972,

Lectures in Mathematical Models of Turbulence, Academic Press, London, England.

Leonard, B. P., 1988, "Simple High-Accuracy Resolution Program for Convective Modelling of Discontinuities," *International Journal of Numerical Method for Fluids*, Vol. 8, pp. 1291～1318.

Van Doormaal, J. P., and Raithby, G. D., 1984, "Enhancements of the SIMPLE Method for Predicting Incompressible Fluid Flows," *Numerical Heat Transfer*, Vol. 7, pp. 147～163.